PHOTONICS Research

Low-noise InGaAs/InP single-photon detector with widely tunable repetition rates

Yan Liang,[1,3] Qilai Fei,[1] Zhihe Liu,[1] Kun Huang,[1] and Heping Zeng[1,2,*]

[1]Shanghai Key Laboratory of Modern Optical Systems, Engineering Research Center of Optical Instruments and Systems, Ministry of Education, School of Optical-Electrical and Computer Engineering, University of Shanghai for Science and Technology, Shanghai 200093, China
[2]State Key Laboratory of Precision Spectroscopy, East China Normal University, Shanghai 200062, China
[3]e-mail: yanliangSPD@163.com
*Corresponding author: hpzeng@phy.ecnu.edu.cn

Received 18 October 2018; revised 12 December 2018; accepted 30 December 2018; posted 2 January 2019 (Doc. ID 348714); published 8 February 2019

InGaAs/InP avalanche photodiodes typically work in the gated Geiger mode to achieve near-infrared single-photon detection. By using ultrashort gates and combining with the robust spike-canceling technique that consists of the capacitance-balancing and low-pass filtering technique, we demonstrate an InGaAs/InP single-photon detector (SPD) with widely tunable repetition rates in this paper. The operation frequency could be tuned conveniently from 100 MHz to 1.25 GHz with the SPD's performance measured to maintain good performance, making it quite suitable for quantum key distribution, laser ranging, and optical time domain reflectometry. Furthermore, the SPD exhibited extremely low-noise characteristics. The detection efficiency of this SPD could reach 20% with the dark count rate of 2.5×10^{-6}/gate and after-pulse probability of 4.1% at 1 GHz.

https://doi.org/10.1364/PRJ.7.0000A1

1. INTRODUCTION

Nowadays, single-photon detectors (SPDs) are employed in more and more applications requiring ultrasensitive detection, such as quantum information processing, nuclear and particle physics, light radar (LIDAR), Raman spectroscopy, biological imaging, and optical time domain reflectometers (OTDRs) [1–7]. In the near-infrared, superconducting nanowire SPDs, upconversion SPDs, and InGaAs/InP avalanche photodiodes (APDs) are the three main techniques for single-photon detection [8–10]. Compared with the other two detectors, InGaAs/InP APDs have relatively poor performance; however, such detectors are widely employed in practical applications for their advantages of compact construction, low power consumption, and low cost [11].

In the free-running mode, the recovery time of the InGaAs/InP APD was required to be long to reduce the error counts, including the after-pulses and dark counts, which limits subsequent high-speed applications. Therefore, InGaAs/InP APDs typically work in the gated Geiger mode to achieve single-photon detection. The gating signals are combined with the dc voltage to control the reverse bias applied on the APD, efficiently decreasing the error counts. In this mode, the operation frequency of the InGaAs/InP SPD is determined by the repetition frequency of the gating signals. We tune the repetition frequency of the gates to change the SPD's working speed. Usually, the gating signals charging and discharging on the APD would inevitably produce the spike noise, making the weak photon-excited avalanche signal difficult to extract. To date, through the unremitting efforts of researchers worldwide, many techniques have been proposed to achieve gigahertz single-photon detection with InGaAs/InP APDs, such as self-differencing, sinusoidal gating, the combination of two aforementioned techniques, low-pass filtering and harmonic subtraction [12–19]. With these techniques, the spike noises could be suppressed down to the thermal noise level. Certainly, there is still room for the improvement of these techniques. For some applications, such as laser ranging and OTDR, it is better to change the operation frequency of the gated SPD for different distance targets.

Another possible application could be exemplified with the measurement-device-independent quantum key distribution, which requires optimizing the working repetition rate for the trade-off between the key production rate and phase-flip error rate [20,21]. However, the sinusoidal gating technique was not suitable for SPDs working at low repetition frequencies; as for the self-differencing technique, the working frequency of the detector was restricted to a fixed and pre-set one, thus degrading its practicability.

In this paper, the InGaAs/InP SPD is demonstrated with widely tunable operation frequency. The ultrashort pulses with adjustable repetition frequencies are used as the gating signals applied on the APD. However, the avalanche time would be shortened, making the amplitude of the avalanche signal decrease and further increasing the difficulty of the extraction. To solve this problem, we use the combining technique that

consists of the capacitance balancing and low-pass filtering to acquire the valid avalanche signals. The spike noise is first subtracted from the output of a mimic capacitance, and then filtered by a low-pass filter (LPF), causing the suppression ratio of the spike noise to exceed 30 dB. Owing to the ultrashort gates and the spike-cancelation technique, the operation frequency of the detector could be tuned continuously over the relatively large range conveniently. Moreover, the error counts, including the dark counts and after-pulses, would decrease with shorter gates [22]. The detection efficiency (DE) of this SPD at 1 GHz could reach 20% with the dark count rate (DCR) of 2.5×10^{-6}/gate and the after-pulse probability of 4.1%.

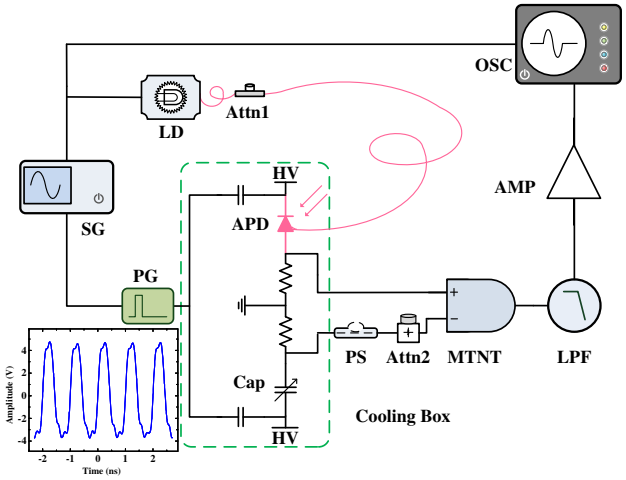

Fig. 1. Schematic setup of the InGaAs/InP SPD with ultrashort gates. SG, signal generator; LD, laser diode; Attn1, variable optical attenuator; PG, pulse-generating module; Cap, adjustable capacitor; PS, phase shifter; Attn2, variable electric attenuator; MTNT, so-called magic-T network consisting of a broadband transformer; LPF, low-pass filter; AMP: RF amplifier; OSC, oscilloscope. Inset, waveform of 1-GHz signal output of the PG.

Finally, while changing the repetition frequency of the gates from 100 MHz to 1.25 GHz, the error counts of the SPD keep at about the same level, ensuring its reliability in the applications of quantum communication, laser ranging, and OTDR.

2. EXPERIMENTAL SETUP

Figure 1 shows the schematic setup of the SPD based on the gated InGaAs/In APD. A pulse-generating module is used to produce ultrashort pulses in order to provide the gating signals of the APD at different frequencies. In the inset of Fig. 1, the waveform of 1-GHz gating signals with the amplitude of ~8 V is exhibited in the oscilloscope (Agilent, DSO9404). The APD is connected in parallel with an adjustable capacitor, which induces an imitative spike. The output signals of the APD and capacitor are connected to the 0 and π inputs of the magic-T network (MTNT), respectively. The differential signal is drawn since the spikes from the two cancel each other. For a good match, a phase shift and an electric attenuator are connected to the output of the adjustable capacitor. The spike suppression ratio of the capacitance-balancing circuit could reach ~20 dB. Figures 2(a) and 2(b) display the oscilloscope trace of the output of the APD and the MTNT, respectively, while 1-GHz ultrashort gates apply on the APD. It could be found that the spike cancelation ratio is not high enough to draw the avalanche signal. We measure the frequency spectrum of the output of the MTNT in Fig. 2(d). The spectral density distribution mainly concentrates on 1 GHz and its harmonic frequencies. Considering the frequency spectrum of the avalanche signal [12,16], an LPF cutting off at 700 MHz is connected to the MTNT. With the attenuation ratio higher than 40 dB at 1 GHz, the spike noise is suppressed down to the thermal noise, and the avalanche signal could be easily obtained, as shown in Fig. 2(c). Before sending the signals into the oscilloscope, a radio frequency (RF) amplifier is employed.

As is well known, the capacitance-balancing technique has been widely used in SPDs under hundreds of megahertz for its

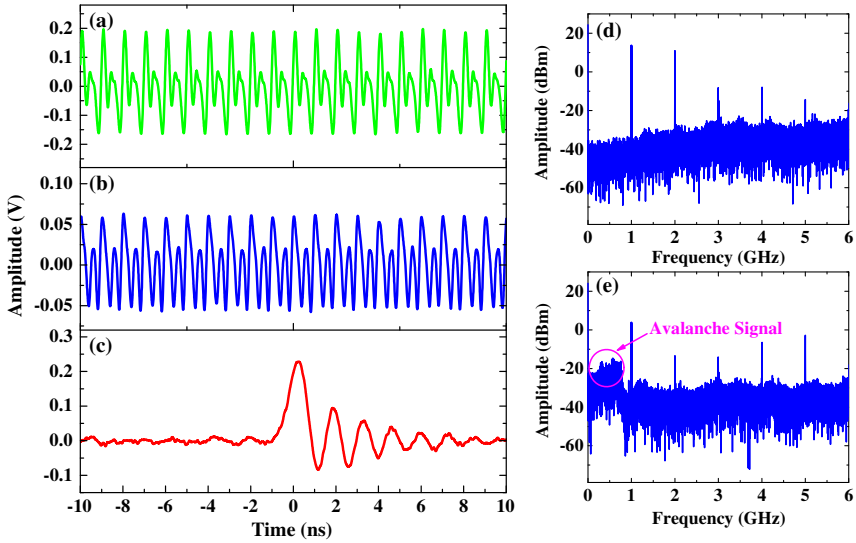

Fig. 2. (a)–(c) Oscilloscope trace of the output of the APD, the MTNT, and the RF amplifier, respectively; (d) and (e) frequency spectrum of the output of the MTNT and the RF amplifier, respectively.

compact construction. And this technique is quite suitable for SPDs with continuously tunable working frequencies. However, its spike suppression ratio needs improvement to be used for high-speed single-photon detection. Since the frequency spectra of the spike noise of gigahertz SPDs are usually higher than gigahertz, we propose to cascade an LPF. An appropriate LPF could sharply eliminate the residual spike while maintaining a great amount of the avalanche signal. In contrast with Fig. 2(d), the distribution of the avalanche signal is much more obvious in Fig. 2(e), ensuring its valid extraction. Besides, it could be seen from Fig. 2(e) that the spike noise has not been completely removed, indicating that the signal-to-noise ratio (SNR) of this SPD can be further perfected. In this schematic, the capacitance-balancing technique, which employs an adjustable capacitor to stimulate the capacitance of the InGaAs/InP APD, is combined with the low-pass filtering technique to achieve robust suppression of the spike noises. The cascaded LPF could not only increase the frequency of the SPD over 1 GHz, but also maintain the performance of the SPD at lower frequencies. With this combining method, we could change the operation frequency continuously from megahertz to gigahertz conveniently.

3. RESULTS AND DISCUSSION

To demonstrate the advantage of the above-mentioned combining technique, we measure the performance of this SPD at different operation frequencies. The InGaAs/InP APD with the effective optical diameter of 25 μm (PGA-300-1, Princeton Lightwave) is Peltier-cooled to work at −30°C to efficiently reduce the dark counts. A fiber-pigtailed pulsed laser diode at 1.55 μm with 50-ps pulse duration is used as the photon source to illuminate the APD. It is synchronously triggered with the gating pulses at 10 MHz and attenuated to contain 0.1 photon per pulse on average. The delay between the laser pulses and the gating pulses is adjusted for the highest DE.

First, this SPD is gated with 100-MHz pulses of 4-V amplitude and a width of less than 1 ns. After the capacitance-balancing circuit and the RF amplifier, the avalanche signal is overlaid on the residual spike and could be gotten by setting a proper threshold level, as shown in the upper part of Fig. 3(a). However, the peak amplitude of the residual spike is beyond 500 mV, which is relatively high, making some buried weak avalanche signals hard to acquire. As mentioned earlier, we could deduce that the frequency spectra of the spike mainly distribute at 100 MHz and its harmonic frequencies. In the setup of the detector, an LPF with cutoff frequency of 700 MHz is used after the capacitance-balancing circuit. The bottom of Fig. 3(b) displays the waveform of the amplified output signal of the LPF. The residual spike is apparently reduced, improving the SNR of the detector.

We change the dc voltage applied on the APD to achieve different DEs and characterize the performance of the SPD. The DCR is measured while the illuminated laser is off. Figure 2(c) shows that there exists an oscillation after the avalanche signal for about 10 ns. Therefore, we set the dead time of this SPD to be 10 ns, which efficiently reduces the error counts caused by the oscillation. Meanwhile, since the after-pulse appears mostly following the avalanche signal, it would decrease drastically as well. The output waveform of the SPD is recorded by the oscilloscope, and the after-pulse probability (AP) could be calculated by the following formula:

$$P_A = \frac{(I_{\mathrm{NI}} - I_D)}{I_{\mathrm{ph}} - I_{\mathrm{NI}}} R, \tag{1}$$

where I_{Ph} and I_{NI} are the count rate per gate at the illuminated and nonilluminated gates, respectively, I_D is the DCR for each gate, and R is the ratio of the repetition frequency of the gating pulse to that of the laser pulse. Here, $R = 10$ is taken. As charted in Fig. 3(b), the DCR and AP increase with the DE, which has been corrected for Poisson statistics of the photons. While the DE is lower than 20%, the DCR and AP have a trend of slow growth. When the DE is adjusted to be 10%, the DCR is calculated to be only 4.0×10^{-7}/gate with the AP of 1.9%, representing the excellent performance of the ultrashort gated InGaAs/InP SPD. With the DE exceeding 20%, the AP begins to rise sharply, limiting the applications of the SPD at 100 MHz.

As the operation frequency increases, the similarity of the capacitance of the APD and the adjustable capacitor deteriorates gradually. The suppression ratio of the capacitance-balancing circuit would inevitably decrease. In the meantime, the avalanche signal would decrease due to the reduction of the duration of the avalanche, making the valid signal hard to get. The previous research suggests that the limiting frequency of the capacitance-balancing technique for single-photon detection was ~700 MHz. Fortunately, we add an LPF in the setup of the SPD. The SNR of the SPD would be improved, especially at relatively high working frequencies. Meanwhile, in consideration of the cutoff frequency of the LPF, we choose to measure the performance of the SPD at 700 MHz to illustrate the superiority of this combining

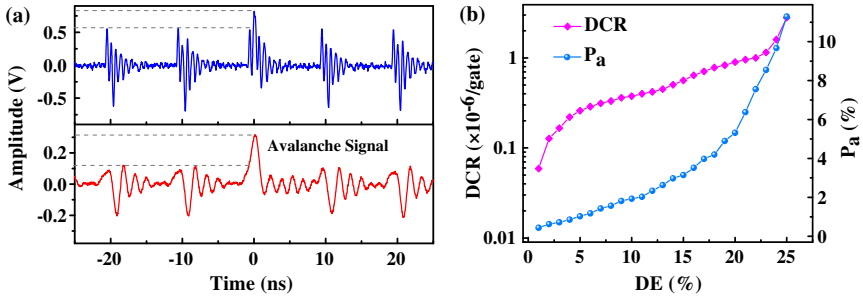

Fig. 3. (a) Waveforms of the amplified output signal of the MTNT and LPF at 100 MHz captured by the oscilloscope in the single mode; (b) DCR and AP as functions of DE of the SPD at 100 MHz.

technique. Figure 4(a) shows the waveform of the amplified output signal of the MTNT and LPF at 700 MHz, respectively. From the upper part, we could see that the avalanche signal is almost entirely buried in the spike. After the LPF, some of the spike that distributes at 700 MHz could be removed partially, while others that distribute at the harmonic frequencies of 700 MHz have been completely canceled. Hence, we could obtain the valid avalanche signal overlaying the spike by setting a proper level, as exhibited in the bottom part of Fig. 4(a). The SNR of the SPD is greatly improved by the LPF. Certainly, more LPFs can be cascaded to further improve the performance of the SPD. Figure 4(b) displays the DCR and AP as functions of DE at 700 MHz. While the DE is less than 10%, the DCR and AP grow slightly and then rise sharply. When the DE increases from 10% to 15%, the DCR increases from 7.1×10^{-7}/gate to 1.4×10^{-6}/gate, whereas the AP witnesses a more significant growth from 3.7% to 7.9%. The AP climbs to be 15.6% with the DE of 20% afterward. Comparing the data with those of the SPD at 100 MHz, the SPD's performance at 700 MHz goes obviously worse. Fortunately, the performance maintains pretty well until the DE exceeds 10%.

With the operation frequency continuing to increase, on account of the different spike suppression ratios of the two techniques, the low-pass filtering technique plays a much more important role than the capacitance-balancing does. For instance, as for 1-GHz SPD, the LPF could eliminate the vast majority of the spike that distributes at 1 GHz and its harmonic frequencies. Here, we test the properties of the SPD at 1 GHz and 1.25 GHz to demonstrate its performance at high operation frequencies. As plotted in Fig. 5(a), the DCR shows a slow upward trend, with DE rising from 1% to 25%. On the whole, the DCR is a little higher at 1.25 GHz than that at 1 GHz. At the DE of 10%, the DCR is 7.9×10^{-7}/gate at 1 GHz and 1.1×10^{-6}/gate at 1.25 GHz, whereas the figure slightly increases to 4.0×10^{-6}/gate at 1 GHz and 4.6×10^{-6}/gate at 1.25 GHz as the DE tunes up to 25%. Figure 5(b) illustrates the AP as a function of the DE. At first, the AP at 1.25 GHz is almost the same as that at 1 GHz while the DE is lower than 20%, increasing quite slowly. Then, the AP begins to rise significantly. For instance, the AP grows dramatically from 4.5% to 18.8% with the DE increasing from 20% to 25% at 1.25 GHz, limiting the applications of the SPD. From the data of Figs. 5(a) and 5(b), we could conclude that the DE of the SPD is preferably no more than 20% to guarantee its reliability.

Comparing with that of the sinusoidally gated InGaAs/In APD [16], we could deduce that the performance of this SPD has been improved due to the use of the ultrashort gates. As is known to all, the ultrashort gates possess shorter pulse width, reducing the time when the bias voltage of the APD is higher than the breakdown voltage. The dark counts and AP would decrease accordingly. However, the amplitude of the avalanche signal would be diminished with the shortening of the avalanche time. On account of the high suppression ratio of the spike noise in the schematic, the extremely weak avalanche signal could be obtained, ensuring the DE of the detector. Here, we register the count rate of the SPD while the delay between optical pulses and the ultrashort gates is scanned to measure the efficient gate width applied on the APD. The dc bias voltage is fixed to maintain the maximum DE of 10%, and the recorded count rate has been normalized. As displayed in Fig. 5(c), the full width at half-maximum of the curve

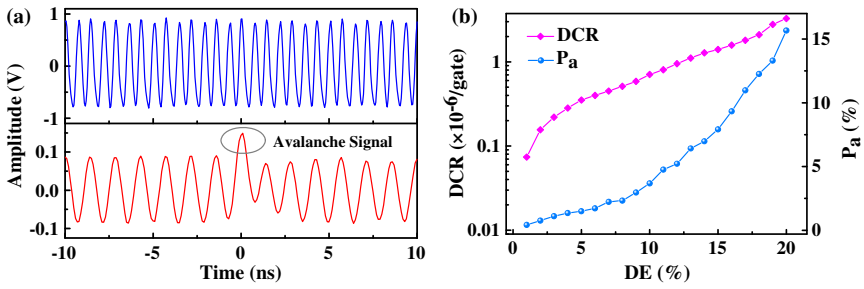

Fig. 4. (a) Waveforms of the amplified output signal of the MTNT and LPF at 700 MHz captured by the oscilloscope in the single mode; (b) DCR and AP as functions of DE of the SPD at 700 MHz.

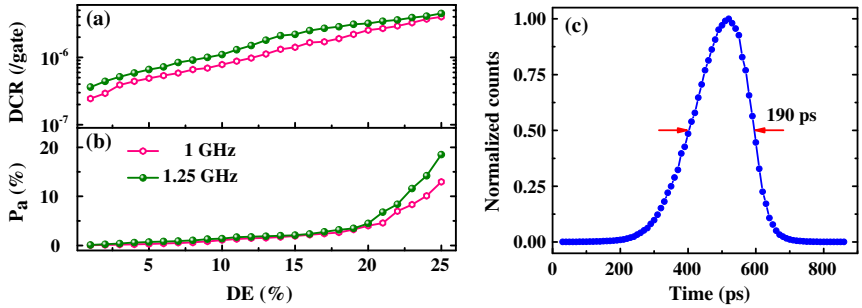

Fig. 5. (a) and (b) DCR and AP as functions of DE of the SPD at 1 and 1.25 GHz; (c) count rate dependent on the laser pulse delay.

indicating the efficient gate width is ~190 ps, which is much shorter than that of the sinusoidal gate. In Ref. [10], the effective gating pulse of the 1.25-GHz sinusoidally gated SPD was measured to be ~125 ps at the DE of 10% with the DCR of $\sim 4.5 \times 10^{-7}$/gate at the same temperature, showing a lower dark noise than that available for this SPD with 165-ps effective gating pulse. To further improve the SPD, we could increase the amplitude and/or narrow the pulse width of the ultrashort gates. It is worth noting that for the sinusoidal gates used in the previous scheme, only the amplitude could be changed. Therefore, the additional degree of freedom in adaptation of the gating pulse duration would offer a broader adjustable range for the SPD over 1 GHz.

4. CONCLUSION

To demonstrate the performance of the ultrashort gated SPD at different operating frequencies at −30°C, we provide an intuitive comparison in Table 1. From the table, we can see that this scheme shows good detecting capability from hundreds of megahertz to gigahertz. When the DE is 20%, the DCR could stay at the level of 10^{-6}/gate, proving that this detection system is capable of realizing the continuous adjustment of the operation frequency over a large range. Certainly, the drawback, which cannot be ignored, is that the AP of the SPD at 700 MHz is quite large when the DE reaches 20%.

Our demonstrated SPD has shown a widely tunable range of operation repetition rates, which combines the capacitance-balancing technique in eliminating the spike noise at relatively lower frequencies and the low-pass filtering technique for higher repetition rates. The performance of the implemented detector degrades at intermediate frequencies of about 700 MHz, which is determined by the cutoff frequency of the LPF to optimize the avalanche signal over gigahertz. At these operation frequencies, the suppression ratio of the capacitance-balancing technique is not high enough to effectively obtain the avalanche signal. To solve this problem, we can replace the tunable capacitor in the capacitance-balancing circuit with a high-speed diode that is more similar to the APD capacitor characteristics to further improve the suppression ratio. On the other hand, it is possible to further optimize its performance by fine-tuning the amplitude and pulse width of the 700 MHz ultrashort gates.

In summary, the ultrashort gated InGaAs/InP APD SPD combines the advantages of both the capacitance-balancing and low-pass filtering techniques to achieve a widely tunable operation frequency range from megahertz to gigahertz, while maintaining excellent detection performance. This SPD could provide a more convenient and reliable detecting solution for applications requiring working at different repetition frequencies, such as quantum key distribution, laser ranging, and OTDR. Furthermore, thanks to the ultrashort pulses and high spike suppression ratio, the property of this SPD is better than that of SPDs using sinusoidal gates. While the 1-GHz ultrashort gate with an efficient gate width of ~190 ps is applied on the APD, the DE of 20% could be finally attained with a DCR of 2.5×10^{-6}/gate and an AP of 4.1%. In this proposal for single-photon detection, the ultrashort pulses are employed to fast-switch the bias voltage of the APD between over-voltage and under-voltage. We could change the amplitude and/or the pulse width to further improve the performance of this SPD, making it applicable in broader fields.

Table 1. Performance of the SPD at Different Repetition Frequencies

	DE of 10%		DE of 20%	
F_{rep}	DCR ($\times 10^{-6}$/gate)	AP	DCR ($\times 10^{-6}$/gate)	AP
100 MHz	0.4	1.9%	0.9	5.3%
700 MHz	0.7	3.7%	3.3	15.7%
1 GHz	0.8	1.2%	2.5	4.1%
1.25 GHz	1.1	1.4%	3.2	4.5%

Funding. National Natural Science Foundation of China (NSFC) (11404212, 11604209, 61127014); National Key Scientific Instrument Project (2012YQ150092); Shanghai Science and Technology Foundation (16JC1400404); Hujiang Foundation of China (D15014).

REFERENCES

1. B. Korzh, C. C. W. Lim, R. Houlmann, N. Gisin, M. J. Li, D. Nolan, B. Sanguinetti, R. Thew, and H. Zbinden, "Provably secure and practical quantum key distribution over 307 km of optical fibre," Nat. Photonics **9**, 163–168 (2015).
2. G. Wang, Z. Y. Li, Y. C. Qiao, Z. Y. Chen, X. Peng, and H. Guo, "Light source monitoring in quantum key distribution with single-photon detector at room temperature," IEEE J. Quantum Electron. **54**, 9300110 (2018).
3. O. Kahl, S. Ferrari, V. Kovalyuk, A. Vetter, G. Lewes-Malandrakis, C. Nebel, A. Korneev, G. Goltsman, and W. Pernice, "Spectrally multiplexed single-photon detection with hybrid superconducting nanophotonic circuits," Optica **4**, 557–562 (2017).
4. B. C. Du, C. K. Pang, D. Wu, Z. H. Li, H. Peng, Y. L. Tao, E. Wu, and G. Wu, "High-speed photon-counting laser ranging for broad range of distances," Sci. Rep. **8**, 4198 (2018).
5. J. Blacksberg, Y. Maruyama, E. Charbon, and G. R. Rossman, "Fast single-photon avalanche diode arrays for laser Raman spectroscopy," Opt. Lett. **36**, 3672–3674 (2011).
6. R. H. Hadfield, "Single-photon detectors for optical quantum information applications," Nat. Photonics **3**, 696–705 (2009).
7. M. Legre, R. Thew, H. Zbinden, and N. Gisin, "High resolution optical time domain reflectometer based on 1.55 μm up-conversion photon-counting module," Opt. Express **15**, 8237–8242 (2007).
8. W. J. Zhang, L. X. You, H. Li, J. Huang, C. L. Lv, L. Zhang, X. Y. Liu, J. J. Wu, Z. Wang, and X. M. Xie, "NbN superconducting nanowire single photon detector with efficiency over 90% at 1550 nm wavelength operational at compact cryocooler temperature," Sci. China: Phys., Mech. Astron. **60**, 120314 (2017).
9. J. H. Ma, X. L. Chen, H. Q. Hu, H. F. Pan, E. Wu, and H. P. Zeng, "Quantum detector tomography of a single-photon frequency upconversion detection system," Opt. Express **24**, 272685 (2016).
10. W. H. Jiang, J. H. Liu, Y. Liu, G. Jin, J. Zhang, and J. W. Pan, "1.25 GHz sine wave gating InGaAs/InP single-photon detector with a monolithically integrated readout circuit," Opt. Lett. **42**, 5090–5093 (2017).
11. M. Stipcevic, B. G. Christensen, P. G. Kwiat, and D. J. Gauthier, "Advanced active quenching circuit for ultrafast quantum cryptography," Opt. Express **25**, 21861–21876 (2017).
12. N. Namekata, S. Adachi, and S. Inoue, "1.5 GHz single-photon detection at telecommunication wavelengths using sinusoidally gated InGaAs/InP avalanche photodiode," Opt. Express **17**, 6275–6282 (2009).

13. Z. L. Yuan, A. W. Sharpe, J. F. Dynes, A. R. Dixon, and A. J. Shields, "Multi-gigahertz operation of photon counting InGaAs avalanche photodiodes," Appl. Phys. Lett. **96**, 071102 (2010).
14. A. Tosi, F. Acerbi, M. Anti, and F. Zappa, "InGaAs/InP single-photon avalanche diode with reduced afterpulsing and sharp timing response with 30 ps tail," IEEE J. Quantum Electron. **48**, 1227–1232 (2012).
15. J. Zhang, R. Thew, C. Barreiro, and H. Zbinden, "Practical fast gate rate InGaAs/InP single-photon avalanche photodiodes," Appl. Phys. Lett. **95**, 091103 (2009).
16. Y. Liang, E. Wu, X. Chen, M. Ren, Y. Jian, G. Wu, and H. Zeng, "Low-timing-jitter single-photon detection using 1-GHz sinusoidally gated InGaAs/InP avalanche photodiode," IEEE Photon. Technol. Lett. **23**, 887–889 (2011).
17. J. C. Campbell, W. Sun, Z. Lu, M. A. Itzler, and X. Jiang, "Common-mode cancellation in sinusoidal gating with balanced InGaAs/InP single photon avalanche diodes," IEEE J. Quantum Electron. **48**, 1505–1511 (2012).
18. A. Restelli, J. C. Bienfang, and A. L. Migdall, "Single-photon detection efficiency up to 50% at 1310 nm with an InGaAs/InP avalanche diode gated at 1.25 GHz," Appl. Phys. Lett. **102**, 141104 (2013).
19. D. Y. He, S. Wang, W. Chen, Z. Q. Yin, Y. J. Qian, Z. Zhou, G. C. Guo, and Z. F. Han, "Sine-wave gating InGaAs/InP single photon detector with ultralow afterpulse," Appl. Phys. Lett. **110**, 111104 (2017).
20. Y. H. Zhou, Z. W. Yu, and X. B. Wang, "Making the decoy-state measurement-device-independent quantum key distribution practically useful," Phys. Rev. A **93**, 042324 (2016).
21. H. L. Yin, T. Y. Chen, Z. W. Yu, H. Liu, L. X. You, Y. H. Zhou, S. J. Chen, Y. Q. Mao, M. Q. Huang, W. J. Zhang, H. Chen, M. J. Li, D. Nolan, F. Zhou, X. Jiang, Z. Wang, Q. Zhang, X. B. Wang, and J. W. Pan, "Measurement-device-independent quantum key distribution over a 404 km optical fiber," Phys. Rev. Lett. **117**, 190501 (2016).
22. X. L. Chen, E. Wu, L. L. Xu, Y. Liang, G. Wu, and H. Zeng, "Photon-number resolving performance of the InGaAs/InP avalanche photodiode with short gates," Appl. Phys. Lett. **95**, 131118 (2009).